



# Intercomparison of in situ NDIR and column FTIR measurements of CO<sub>2</sub> at Jungfrauoch

Michael F. Schibig<sup>1,a</sup>, Emmanuel Mahieu<sup>2</sup>, Stephan Henne<sup>3</sup>, Bernard Lejeune<sup>2</sup>, and Markus C. Leuenberger<sup>1</sup>

<sup>1</sup>Climate and Environmental Physics, Physics Institute and Oeschger Centre for Climate Change Research, University of Bern, Bern, Switzerland

<sup>2</sup>Institut d'Astrophysique et de Géophysique, Université de Liège, Liège, Belgium

<sup>3</sup>Empa, Swiss Federal Laboratories for Materials Testing and Research, Dübendorf, Switzerland

<sup>a</sup>now at: National Oceanic and Atmospheric Administration, Earth System Research Laboratory, Boulder, CO 80305, USA

Correspondence to: Markus C. Leuenberger (leuenberger@climate.unibe.ch)

Received: 9 February 2016 – Published in Atmos. Chem. Phys. Discuss.: 16 March 2016

Revised: 8 July 2016 – Accepted: 14 July 2016 – Published: 8 August 2016

**Abstract.** We compare two CO<sub>2</sub> time series measured at the High Alpine Research Station Jungfrauoch, Switzerland (3580 m a.s.l.), in the period from 2005 to 2013 with an in situ surface measurement system using a nondispersive infrared analyzer (NDIR) and a ground-based remote sensing system using solar absorption Fourier transform infrared (FTIR) spectrometry. Although the two data sets show an absolute shift of about 13 ppm, the slopes of the annual CO<sub>2</sub> increase are in good agreement within their uncertainties. They are  $2.04 \pm 0.07$  and  $1.97 \pm 0.05$  ppm yr<sup>-1</sup> for the FTIR and the NDIR systems, respectively. The seasonality of the FTIR and the NDIR systems is  $4.46 \pm 1.11$  and  $10.10 \pm 0.73$  ppm, respectively. The difference is caused by a dampening of the CO<sub>2</sub> signal with increasing altitude due to mixing processes. Whereas the minima of both data series occur in the middle of August, the maxima of the two data sets differ by about 10 weeks; the maximum of the FTIR measurements is in the middle of January, and the maximum of the NDIR measurements is found at the end of March. Sensitivity analyses revealed that the air masses measured by the NDIR system at the surface of Jungfrauoch are mainly influenced by central Europe, whereas the air masses measured by the FTIR system in the column above Jungfrauoch are influenced by regions as far west as the Caribbean and the USA.

The correlation between the hourly averaged CO<sub>2</sub> values of the NDIR system and the individual FTIR CO<sub>2</sub> measurements is 0.820, which is very encouraging given the largely different sampling volumes. Further correlation analyses showed, that the correlation is mainly driven by the an-

nual CO<sub>2</sub> increase and to a lesser degree by the seasonality. Both systems are suitable to monitor the long-term CO<sub>2</sub> increase, because this signal is represented in the whole atmosphere due to mixing.

## 1 Introduction

CO<sub>2</sub> is the most important anthropogenic greenhouse gas, with a large contribution to the greenhouse effect (Arrhenius, 1896) and an additional radiative forcing of the atmosphere currently evaluated at  $1.68 \text{ W m}^{-2}$  (IPCC, 2013). The strength of the forcing depends on its atmospheric mole fraction, which is ruled by the processes of the carbon cycle as well as by anthropogenic CO<sub>2</sub> emissions from fossil fuel combustion and land use change. The major reservoirs of the carbon cycle besides the lithosphere are the soils, the ocean, the biosphere and the atmosphere, where the latter is also acting as the main link between the biosphere and the ocean. The linking process between the atmosphere and the ocean is dissolution of CO<sub>2</sub> in oceanic water, where it is subsequently chemically bound to bicarbonate and carbonate and therefore removed from the carbon cycle on a longer timescale (Broecker and Peng, 1982; Feely et al., 2004; Heinze et al., 1991; Sillén, 1966). The processes coupling the biosphere with the atmosphere are photosynthesis, where CO<sub>2</sub> is taken up by plants, and respiration, where CO<sub>2</sub> is released back to the atmosphere. Photosynthesis and respiration are mainly driven by climatic conditions of the envi-

ronment. In the Northern Hemisphere, especially in the extratropics with distinct seasons, the dominating process in late spring, summer, and autumn is photosynthesis and thereby the uptake of CO<sub>2</sub> from the atmosphere. In autumn respiration and with it the release of CO<sub>2</sub> from the biosphere into the atmosphere starts to take over and is the ruling process in winter until spring when photosynthesis becomes the dominating process again. Due to these alternating processes, the CO<sub>2</sub> mole fraction in the atmosphere shows a seasonal cycle with its maximum generally in early spring and its minimum in autumn (Halloran, 2012; Keeling et al., 1976, 2001; Machida et al., 2002). A further component in the change of atmospheric CO<sub>2</sub> mole fraction is CO<sub>2</sub> release due to fossil fuel combustion (Karl and Trenberth, 2003; Revelle and Suess, 1957; Tans et al., 1990). Presently, roughly half of the anthropogenically produced CO<sub>2</sub> ends up in the oceans and the biosphere, whereas the other half is accumulating in the atmosphere and leads to a more or less steady increase of the atmospheric CO<sub>2</sub> mole fraction (Bender et al., 2005; Le Quéré et al., 2014; Sabine et al., 2004). Measuring the atmosphere's CO<sub>2</sub> mole fraction on the long-term is therefore important to understanding the sources and sinks of the carbon cycle and the annual CO<sub>2</sub> increase due to fossil fuel combustion and land use change. To measure the evolution of CO<sub>2</sub> in the atmosphere on a global-scale satellite remote sensing methods can be used, such as OCO-2 (Crisp et al., 2004; Pollock et al., 2010; Thompson et al., 2012) or GOSAT (Chevallier et al., 2009; Yokota et al., 2009), but they are limited by cloud cover, temporal coverage due to the orbit, coarse resolution, etc. An intercomparison between GOSAT and several TCCON (Total Carbon Column Observation Network) stations showed a mean difference for daily averages of  $-0.34 \pm 1.37$  ppm (Heymann et al., 2015). Ground-based measurement systems on the other hand have a high temporal resolution and provide very accurate data, which can be used to validate satellite data (Buchwitz et al., 2006; Butz et al., 2011; Dils et al., 2006; Morino et al., 2011; Wunch et al., 2011) or as model input (Chevallier et al., 2010), but surface observations have often a limited representativeness and are often influenced by nearby processes and hence not representative for larger areas. Also the influence of the biosphere or anthropogenic pollution can be a serious issue and make it very challenging to measure background air. Therefore, to measure global CO<sub>2</sub> trends the sampling site should be at a very remote place such as Mace Head Station (Bousquet et al., 1996; Messenger et al., 2008) on the western coast of Ireland or the flask sampling network in the Pacific of NOAA (Komhyr et al., 1985; Trolrier et al., 1996). Another possibility is to measure in the free troposphere, e.g., with airplanes as was done in the CARIBIC project (Brenninkmeijer et al., 2007) or the CONTRAIL project (Machida et al., 2008) or at high altitudes that are mostly in the free troposphere such as Mauna Loa (Keeling et al., 1976, 1995; Pales and Keeling, 1965; Thoning et al., 1989). The High Alpine Research Station Jungfraujoch (JFJ) with its altitude of 3580 m a.s.l.

(Sphinx Observatory) and position mostly above the planetary boundary (Henne et al., 2010) is therefore a very suitable spot to conduct ground-based CO<sub>2</sub> background measurements.

The University of Liège (Belgium) has been measuring infrared radiation at JFJ since the 1950s and started regular Fourier transform infrared (FTIR) measurements in 1984. The Climate and Environmental Physics Division (KUP) of the University of Bern started measuring CO<sub>2</sub> and  $\delta\text{O}_2/\text{N}_2$  in 2000 with a flask sampling program and since the end of 2004, CO<sub>2</sub> and O<sub>2</sub> have been additionally measured with a continuously operating system of a nondispersive infrared analyzer (NDIR) and a paramagnetic cell. In this study we compared the FTIR and the NDIR data set to see if the two complementary measurement techniques are catching the same trends, seasonalities and variations in atmospheric CO<sub>2</sub> mole fraction at and above Jungfraujoch.

## 2 Methods

### 2.1 Measurement site

The High Altitude Research Station Jungfraujoch (JFJ) is located 7°59'02" E, 46°32'53" N at the northern margin of the Swiss Alps. The Jungfraujoch is a mountain saddle between the Mönch (4099 m a.s.l.) and Jungfrau (4158 m a.s.l.) summits at a height of 3580 m a.s.l. (Sphinx Observatory) and is accessible year-round by train. Because of the high elevation, the station is usually above the planetary boundary layer (PBL) and therefore mainly receives air from the free troposphere, which is why it was classified as "mostly remote" by Henne et al. (2010). Nevertheless, the station can be influenced by polluted air during specific events such as frontal passages and Föhn (Uglietti et al., 2011; Zellweger et al., 2003) or thermal uplift of polluted air from the surrounding valleys on fair weather days (Baltensperger et al., 1997; Henne et al., 2005; Zellweger et al., 2000). Because of the high elevation, the accessibility and the good infrastructure, the JFJ is an ideal location for in situ measurements of atmospheric background air from continental Europe (Baltensperger et al., 1997; Henne et al., 2010; Zellweger et al., 2003). JFJ is also one of the currently 29 core sites of the WMO GAW (Global Atmospheric Watch) programme.

### 2.2 In situ NDIR measurements at Jungfraujoch

The KUP CO<sub>2</sub> measurements are based on a combined system to monitor CO<sub>2</sub> and O<sub>2</sub> changes in the atmosphere. The ambient air is entering through a strongly ventilated ( $600 \text{ m}^3 \text{ h}^{-1}$ ) common inlet on the observatory's roof to a manifold, which serves many trace gas analyzers, where an aliquot of it is drawn to the KUP system. The air is cryogenically dried to a dew point of  $-90^\circ\text{C}$  (FC-100D21, FTS systems, USA). Temperature as well as pressure is stabilized to avoid influences caused by ambient air density fluctua-

tions. This allows for the determination of CO<sub>2</sub> by a NDIR spectrometer (Maihak S710) measuring at a wavelength of 4.26 μm with a frequency of 1 Hz and O<sub>2</sub> by a paramagnetic cell under highly controlled conditions. Measurements are done in a cyclic sequence of 18 h with each gas measured for 6 min with only the last 115 s of a 6 min period used for mole fraction determination, to allow for signal stabilization after changing the sample source. At the beginning of each 18 h sequence, the system is calibrated with two reference gases (high and low span). A working gas is measured between two ambient air measurements to correct for short-term variations. All measurements ending in a particular hour are used for the calculation of hourly mean CO<sub>2</sub> observations, which in our case includes therefore six ambient observation values per hour. Cylinder measurements with a known mole fraction showed a long-term precision for hourly averages better than 0.04 ppm. The accuracy of our target cylinder corresponds to less than 0.1 ppm (WMO target value for CO<sub>2</sub> measurements) calculated as standard deviation of the mean considering the number of independent calibration set (high span, low span, working gas). The CO<sub>2</sub> values are reported on the WMO X2007 scale. A multi-annual intercomparison between the NDIR system and a cavity ring-down spectroscope at JFJ showed a very good agreement of the CO<sub>2</sub> measurements (Schibig et al., 2015).

### 2.3 Column FTIR measurements at Jungfraujoch

The University of Liège has been recording atmospheric solar spectra at JFJ since the early 1950s. The current FTIR instrument is a commercially available Bruker IFS-120 HR with a resolution of up to 0.001 cm<sup>-1</sup> (Mahieu et al., 1997). It features interchangeable detectors, a KBr beam-splitter and dedicated optical filters, which altogether give the possibility to cover the 1 to 14 μm spectral range (Zander et al., 2008). Here gases such as CO<sub>2</sub>, CH<sub>4</sub>, and H<sub>2</sub>O show numerous absorption lines documenting contributions to the greenhouse effect. These spectra also contain information about the abundance of many additional absorbing gas species in the path between the instrument and the sun, essentially present either in the troposphere or in the stratosphere. The CO<sub>2</sub> data set used here has been derived from the reference total column time series produced within the framework of the NDACC monitoring program (Network for the Detection of Atmospheric Composition Change; see <http://www.ndacc.org>), presented previously in, e.g., Zander et al. (2008; see Fig. 6). In the meantime, the data set has been consistently updated, still using the SFIT-1 algorithm (version 1.09c) and a single microwindow spanning the 2024.3–2024.7 cm<sup>-1</sup> spectral interval, whose main spectral line at 2024.564 cm<sup>-1</sup> is coming from <sup>13</sup>CO<sub>2</sub>. The uncertainty range on the strength of this CO<sub>2</sub> line is estimated at 2 to less than 5 % in the HITRAN compilation (Rothman et al., 2005), leading to a systematic error on the retrieved total column of the same magnitude. The single CO<sub>2</sub> a priori vertical distribution used in

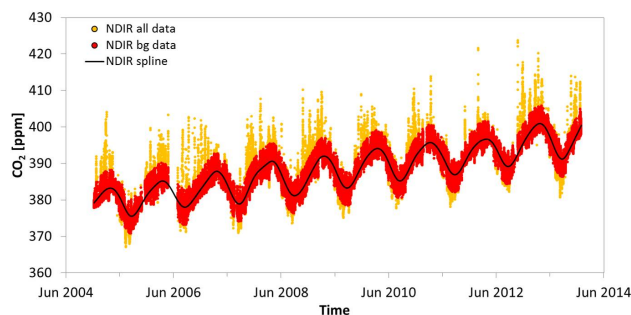


**Figure 1.** In situ CO<sub>2</sub> mole fractions of the NDIR measurements as a function of time in ppm at JFJ: all hourly averages before filtering (yellow), hourly averages after filtering (red), and the spline (black line). Note that the yellow points correspond to only about 5 % of the whole data set.

all retrievals is characterized by a constant mixing ratio of 338 ppm from the surface up to the tropopause, then slightly decreasing to stabilize at 330 ppm at 20 km and above. During the retrieval process, a simple scaling of the whole vertical profile is performed, accounting for interferences by weak ozone and water vapor lines, and the mixing ratio derived for CO<sub>2</sub> in the troposphere is used in the present comparisons. Note that the representativeness of this unique profile is not optimal for all seasons and may lead to an underestimation of the seasonal amplitude (see Fig. 1 in Barthlott et al., 2015), because of a non-optimum vertical sensitivity of the FTIR retrieval. Indeed, typical values of the total column averaging kernel – indicative of the fraction of information coming from retrieval rather than from the a priori (e.g., Vigouroux et al., 2015) – are in the 0.5–1 range between the ground and 10 km altitude, in line with Fig. 4 of Barthlott et al. (2015). Over all the standard deviation of multiple measurements over the course of a single day corresponds to less than one ppm, which is significantly smaller than the observed seasonal cycle.

### 2.4 Data processing

The NDIR data set is much more influenced by near-ground processes, such as thermal uplift of PBL air from the surrounding valleys, advection of PBL air by synoptic events, etc., than the FTIR and shows therefore a higher variability. Additionally, because of the large volume of the column sampled by the FTIR above JFJ the CO<sub>2</sub> mole fraction measured by the FTIR is averaged and the data set is far less sensitive to local events than the in situ NDIR measurements. The FTIR needs a cloudless sky to be able to measure, whereas the NDIR system is measuring under all conditions, which can lead to very high CO<sub>2</sub> mole fractions during, e.g., Föhn events, when the sky is cloudy and polluted air from the heavily industrialized Po basin (northern Italy) is advected to JFJ. Therefore, only measurements of background air should be taken into account to compare the two data sets properly.

### 2.4.1 Filtering, trend, and seasonality calculation

The background data were selected using a statistical approach. A cubic spline was fitted to both data sets individually, the standard deviation of the residuals was calculated and all points beyond  $2.7\sigma$  were flagged as outliers. This process was repeated in both data sets until convergence. The threshold of  $2.7\sigma$  was chosen because in normally distributed data more than 99 % of the total data points would be included for further calculations and only the most obvious outliers (less than 1 %) would be rejected.

The CO<sub>2</sub> mole fraction is dominated by two major processes. One is the linear increase due to fossil fuel combustion (trend) and one is the annual increase and decrease due to respiration and photosynthesis, and to a lesser degree due to fossil fuel combustion (seasonality). The trend was calculated for both data sets individually with a Monte Carlo approach.

For the trend calculation we intentionally used the data sets including seasonal signals because it leads to realistic trend error estimates compared to deseasonalized data sets, which in our view tend to underestimate the error. The data sets were split in two subsets, where each of the subsets spanned over  $n - 0.5$  phases (in this study  $n$  equals 9 years) to prevent a bias in the trend calculation due to the seasonal cycle. The first subset started in January 2005, the second subset started in July 2005. In each subset about 2 % (a higher number does improve the result) of the points were selected randomly and the linear trend was calculated. This was repeated 500 times with each subset and the averages of these linear trends were taken as the slopes of the data sets.

To calculate the seasonality, the two data sets were detrended and monthly averages were formed, from which the seasonality was calculated as the difference between the highest and the lowest value.

### 2.4.2 Correlation analysis

Because of the different time resolutions for in situ and FTIR measurements, we selected those in situ measurements (6 min and hourly NDIR averages) that are closest ( $\pm 30$  min) to the FTIR values for correlation analysis.

Since the differences between both correlation analyses were negligible (see results section), it was decided to continue with the hourly averages of the NDIR data set only, which is the common output of the NDIR database.

The FTIR's sample volume is much bigger than the NDIR system's and because of transportation processes there is a possibility of mixing processes. To check, a moving average of the NDIR data with increasing width was calculated to see if the correlation is enhanced with expanding width (from 0 to  $\pm 600$  h).

Furthermore, the column measurements were retrieved for the layer between 3.58 km (altitude of the Sphinx Observatory) to the top atmosphere (set to 100 km in the retrieval

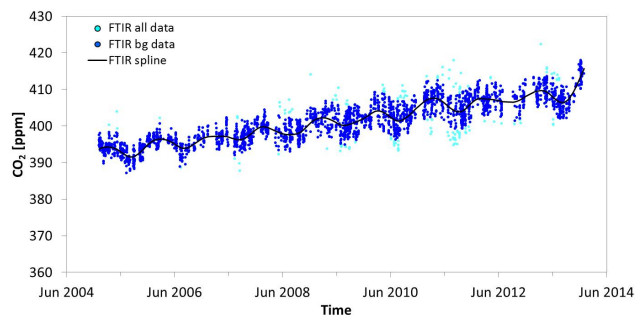


**Figure 2.** CO<sub>2</sub> mole fractions of the FTIR measurements as a function of time in ppm in the column above JFJ: all hourly averages before filtering (light blue), hourly averages after filtering (dark blue), and the spline (black line). The light blue points correspond to about 5 % of the whole data set.

scheme), whereas the NDIR system is measuring at the lower boundary of the FTIR's sampling column; therefore, it is possible that a time shift in the measured CO<sub>2</sub> mole fractions, due to advection, uplift of air parcels, etc., occurs. To check whether a systematic time shift exists between the two data sets, the NDIR measurements were shifted relative to the FTIR data from  $-60$  to  $+60$  days (corresponding to  $-1440$  to  $+1440$  h) in hourly steps and again the correlation of the two data sets was calculated. If there is a systematic time shift, the deviation should be indicated by increased correlation values.

### 2.5 FLEXPART model runs

From 2009 to 2011, backward Lagrangian particle dispersion model simulations were performed with FLEXPART (Stohl et al., 2005) to simulate the transport towards JFJ and estimate surface source sensitivities (footprints) of the sampled air masses. To account for the complex flow in the Alpine area, a regional-scale version of the model driven by operational output from the regional-scale numerical weather prediction model COSMO as produced by MeteoSwiss was used (Henne et al., 2016; Oney et al., 2015). Since COSMO is a limited area model, the transport of particles leaving the domain was further simulated in the global-scale version of FLEXPART (Stohl et al., 2005) driven by operational analysis fields of the European Centre for Medium Range Weather Forecast (ECMWF). In the Alpine area, COSMO input data had a horizontal resolution of approximately  $2 \text{ km} \times 2 \text{ km}$ , in western Europe  $7 \text{ km} \times 7 \text{ km}$ . Of the 1214 FTIR measurements in this period, footprints were available for 766. The model simulated footprints of the surface in situ observations and five partial columns above JFJ reaching from 3365–4226, 4226–4912, 4912–5629, 5629–6386, and 6386–7184 m a.s.l. The lower boundary is below JFJ in order to account for smoothed model topography. Particles released at and above JFJ were followed 10 days backward in time by simulating atmospheric transport by the mean wind, turbu-



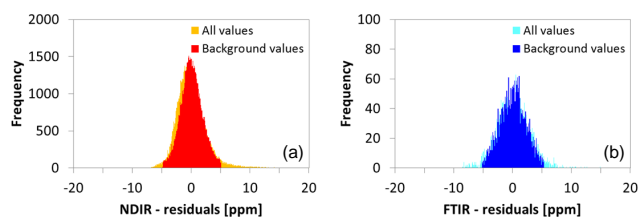


**Figure 3.** (a) Histogram of all NDIR residuals (yellow) and the filtered NDIR residuals representing the background values (red) of the in situ measurements; (b) histogram of all FTIR residuals (light blue) and the filtered FTIR residuals representing the background values (blue) of the column.

lence, and convection. Along the integration the particle positions were evaluated every 3 h to derive particle residence times close to the surface (0 to 100 m a.g.l. – above model ground). The residence times give a direct link between concentrations at the receptor (here location of observations) and a source on the evaluated output grid. Hence, residence times are also often termed source sensitivities or concentration footprints. For individual backward simulations total residence times were calculated by summation over all transport integration steps. Larger total residence times usually indicate a larger probability that an air mass was influenced by fluxes at the Earth's surface, whereas lower values indicate air masses that mainly resided in the free troposphere prior to arrival at the receptor. Surface residence times were evaluated on regular longitude–latitude grids. The resolution was  $0.5^\circ \times 0.5^\circ$  globally,  $0.2^\circ \times 0.2^\circ$  over Europe and an even higher resolution of  $0.1^\circ \times 0.1^\circ$  was used in the Alpine area. The surface residence times corresponding to each measurement and each partial column were averaged to monthly means to get information about the origin of the air masses in the according month (Henne, unpublished data; Henne et al., 2013). Further summation over all land cells in the output grid gives an integrating parameter for potential surface influence.

### 3 Results

Because of the different measurement techniques, the number of data points in the two data sets is different. In the period 2005 to 2013 the NDIR data set contains 68 477 hourly averages from which about 5 % were omitted as pollution or depletion events resulting from PBL influence as estimated by the filtering (Fig. 1). In the same period, the FTIR data set shows 3068 measurements of which about 5 % were rejected as pollution and depletion events, too (Fig. 2). For all further calculations, only the filtered data sets were used.

The average of the detrended and deseasonalized NDIR data before and after filtering was  $0.00 \pm 2.65$  and  $0.00 \pm 1.84$  ppm (Fig. 3a), the average of the FTIR data was  $0.01 \pm 2.61$  and  $0.01 \pm 2.16$  ppm, respectively (Fig. 3b).

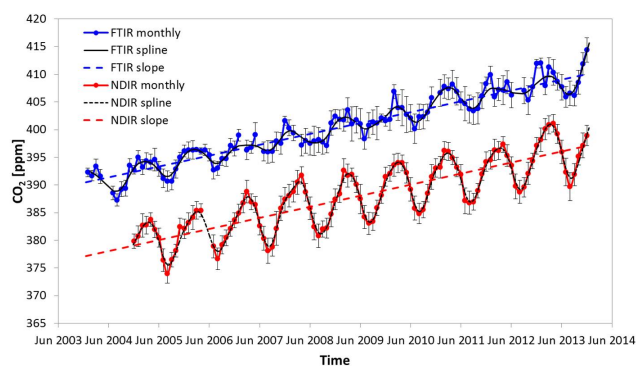


**Figure 4.** FTIR and NDIR CO<sub>2</sub> measurements at JFJ as a function of time: monthly averages of the filtered FTIR data (blue), spline (black line), the annual CO<sub>2</sub> increase calculated from the filtered FTIR data set (blue dashed line), monthly averages of the filtered NDIR data (red), spline (black dotted line), and the annual CO<sub>2</sub> increase calculated from the filtered NDIR data set (red dashed line).

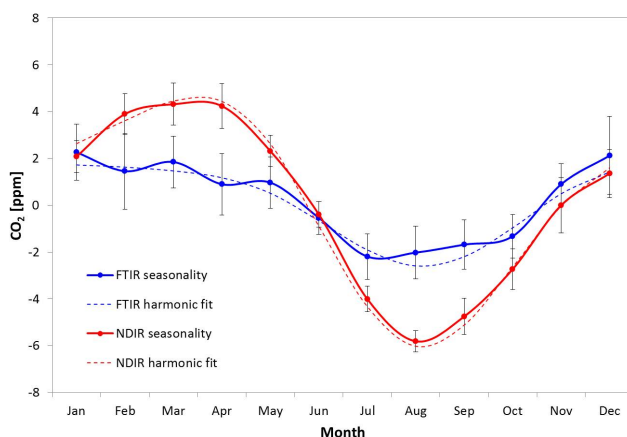


**Figure 5.** Monthly averaged seasonality of the filtered FTIR and NDIR CO<sub>2</sub> measurements for the 9 years of the comparison: averaged NDIR seasonality (red), two harmonic fit of the NDIR seasonality (red dashed line), averaged FTIR seasonality (blue), and two harmonic fit of the FTIR seasonality (dashed blue line).

With a Monte Carlo algorithm, the values of the annual change of the CO<sub>2</sub> mole fraction of the two data sets were calculated. Despite the shift between the two data sets of roughly 13 ppm and the different measurement techniques the annual CO<sub>2</sub> increase is quite similar. The FTIR slope is  $2.04 \pm 0.07$  ppm yr<sup>-1</sup> and the NDIR data set shows a slope of  $1.97 \pm 0.05$  ppm yr<sup>-1</sup>, so they are equal within their uncertainties (Fig. 4). The observed offset between the FTIR (NDACC) and in situ records at Jungfraujoch contrasts the comparison of NDACC and TCCON records as determined at Ny-Ålesund, which do not show any offset at all when using several individual CO<sub>2</sub> lines for the mid-IR (2000 to 4000 cm<sup>-1</sup>) (Buschmann et al., 2016). However, the FTIR–NDIR offset of about 3 % is commensurate with the systematic uncertainty affecting the FTIR measurement; see Sect. 2.3.

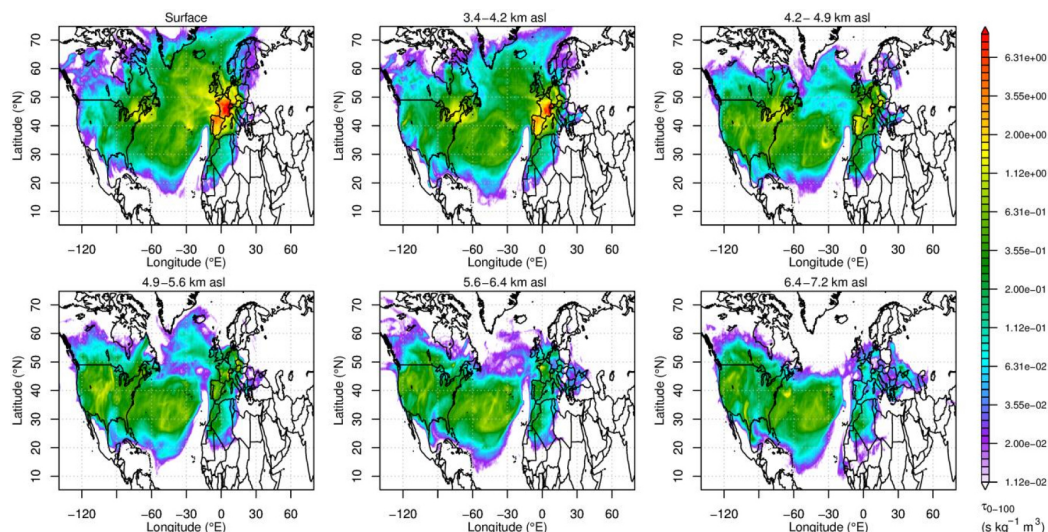


**Figure 6.** Surface source sensitivity (footprints) of the air masses at JFJ (surface in situ) and in the sub-columns above JFJ in August ( $\text{CO}_2$  minimum of FTIR and NDIR time series) in the period 2009 to 2011 simulated with FLEXPART. The height of the sub-columns is given above the according subplots, the x axis is the longitude, the y axis represents the latitude, the color code of the sensitivity is given at the right side.

By detrending the data sets with the derived slopes, the seasonality can be calculated. The column data set shows a seasonality of  $4.46 \pm 1.11$  ppm, whereas the in situ measurements at the Sphinx Observatory show a seasonality roughly twice as big, namely  $10.10 \pm 0.73$  ppm. To find the moment of the average minima and maxima, a two harmonic fit function was applied to the detrended data sets. The minima of the FTIR and NDIR data sets are both in the middle of August, but the maxima are roughly 10 weeks apart. The maximum of the NDIR data sets occurs at the end of March, whereas seasonality of the FTIR data set already reaches its maximum in the middle of January (Fig. 5).

The footprints of August, January, and March, when the extrema of the seasonal cycle occurred, as calculated with FLEXPART show that the in situ observation at Jungfraujoch is mainly receiving air masses that are influenced by central Europe, and to a lesser degree by the Mediterranean area and the northern Atlantic (Figs. 6, 7 and 8).

With increasing altitude, the footprints of the sub-columns indicate, that the measured air masses become more sensitive to regions as far west as, e.g., the Caribbean and the USA and that the influence from the European continent and northern regions higher than  $50^\circ$  N is decreasing (Figs. 6, 7 and 8).

In general, the decoupling between the FTIR columns and possible surface fluxes of  $\text{CO}_2$  from land surfaces north of  $30^\circ$  N was the strongest during the winter month (January to March), when especially low surface residence times were simulated by FLEXPART for the free tropospheric FTIR columns (Fig. 9). From April to September larger surface residence times were seen also for the FTIR columns and a stronger coupling between surface fluxes and the free tro-

posphere can be expected. At the same time residence times over tropical land surface (south of  $30^\circ$  N) were generally larger for the FTIR columns compared to the surface and were especially increased from February to April (see Fig. 9).

To estimate the relationship between the FTIR and NDIR measurements the correlation was calculated. The FTIR measurements take normally about 10 min and are done whenever possible. Therefore, the FTIR data are reported exactly at the measuring time. The NDIR on the other hand is measuring non-stop, but only 115 s of 6 min intervals (see methods) are used to calculate a data point and the 6 min data are normally averaged to hourly averages. Therefore, we first checked whether the high-resolution data are necessary or hourly data are good enough. To do so, to each FTIR data point the nearest high resolution and hourly averaged NDIR values were assigned. An additional condition was that the NDIR value must not be further apart than  $\pm 30$  min, otherwise no NDIR data point was set, which was the case in about 10 % of the FTIR data points. The correlation between the FTIR and the high-resolution NDIR  $\text{CO}_2$  measurements and between the FTIR and the hourly averages were calculated to be 0.819 and 0.820, respectively, so the differences between the two regression values are negligible. To examine the relationship between the FTIR and the NDIR measurements further, the seasonality of the two data sets was eliminated, which gave almost the same correlation of 0.824 (0.838 with the high-resolution data). In the next step, only the trend was subtracted and the remaining seasonalities were compared, which lead to a much smaller correlation of 0.460 (0.461 with the high-resolution data). In a final step, the trend as well as the seasonality was removed, which resulted in a



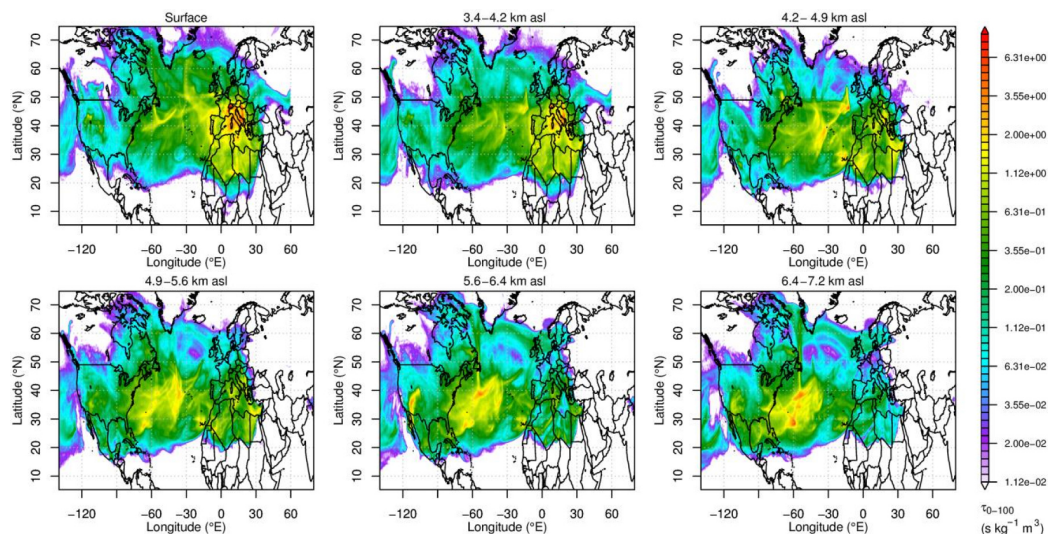


**Figure 7.** Surface source sensitivity (footprints) of the air masses at JFJ (surface in situ) and in the sub-columns above JFJ in January ( $\text{CO}_2$  maximum of the FTIR data set) in the period 2009 to 2011 simulated with FLEXPART. The height of the sub-columns is given above the according subplots, the  $x$  axis is the longitude, the  $y$  axis represents the latitude, the color code of the sensitivity is given at the right side.

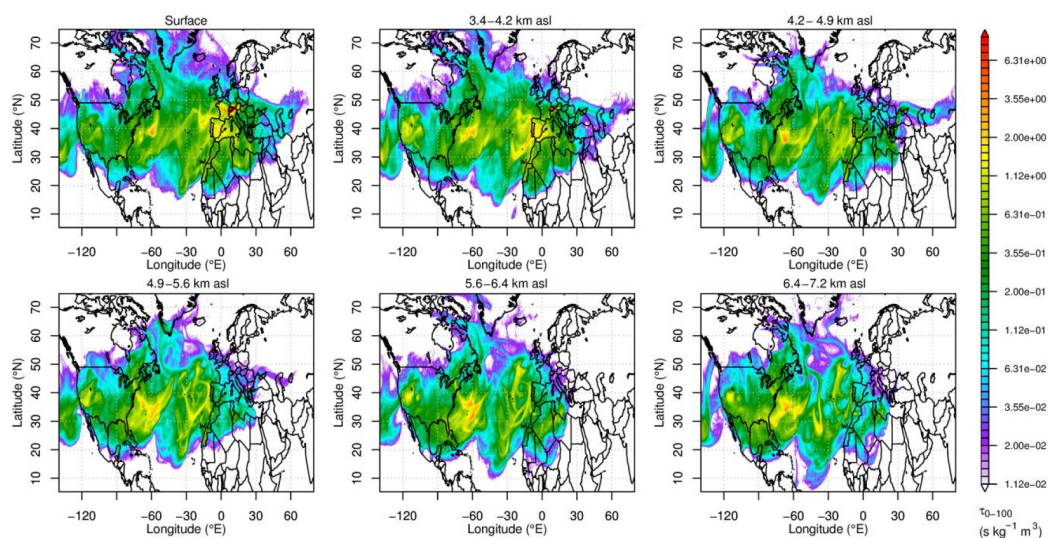


**Figure 8.** Surface source sensitivity (footprints) of the air masses at JFJ (surface in situ) and in the sub-columns above JFJ in March ( $\text{CO}_2$  maximum of the NDIR data set) in the period 2009 to 2011 simulated with FLEXPART. The height of the sub-columns is given above the according subplots, the  $x$  axis is the longitude, the  $y$  axis represents the latitude, the color code of the sensitivity is given at the right side.

correlation of 0.071 (0.084 high-resolution data vs. FTIR). Since correlations between the FTIR data and the NDIR's high-resolution and the hourly data were almost the same, only the hourly data were considered for further calculations (Fig. 10).

As mentioned above, the column measurements represent the whole vertical distribution above Jungfraujoch whereas the NDIR system is measuring at the base of the FTIR's sampling column. Therefore, the two records might be time delayed due to advection, uplift of air parcels, etc. To check for a potential time lag, the NDIR measurements were shifted

relative to the FTIR data from  $-1440$  to  $+1440$  h in hourly steps.

The correlations between the NDIR and FTIR data sets and between the deseasonalized NDIR and FTIR data sets show a peak region at a time shift from  $-10$  to  $60$  h with the highest correlation being 0.830 and 0.836, respectively (Fig. 11a, b). The correlation between the data sets is decreasing before and after this range, in the deseasonalized data sets the correlation stays more or less stable. The correlation between the two trend-corrected data sets shows a plateau of enhanced correlation values from  $-50$  to  $200$  h

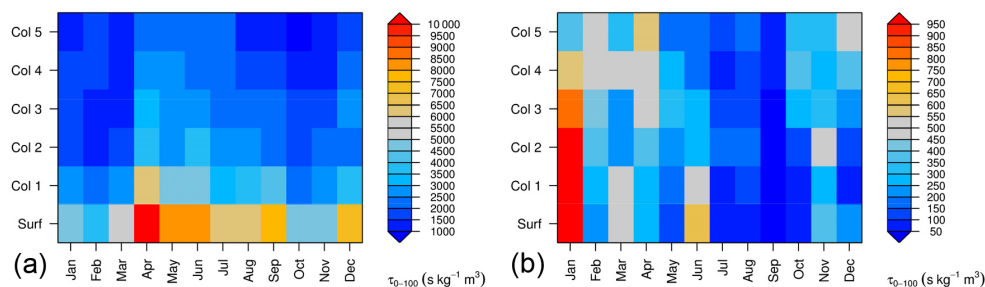


**Figure 9.** Annual cycle of FLEXPART-derived total surface residence time over land for different vertical arrival columns above Jungfraujoch: (left) for land surfaces north of 30° N and (right) for land surfaces south of 30° N.

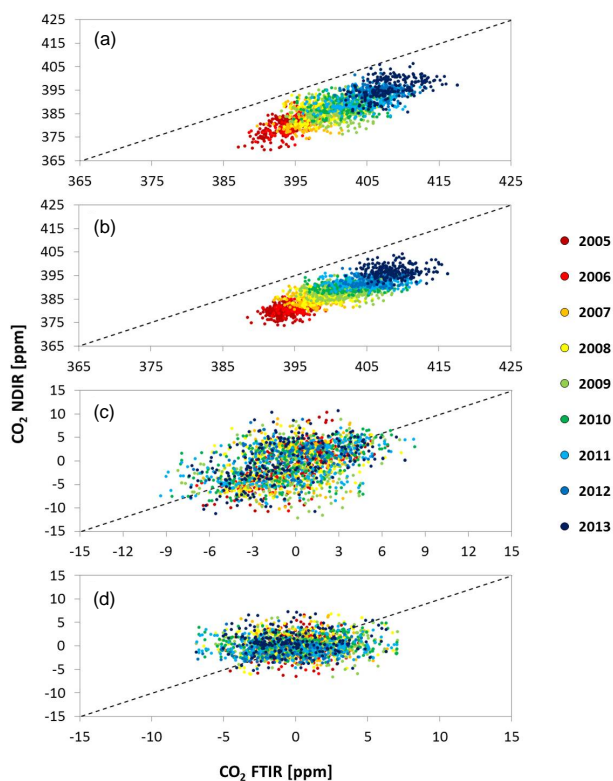


**Figure 10.** Correlation plots of the filtered hourly NDIR CO<sub>2</sub> measurements vs. the filtered FTIR CO<sub>2</sub> measurements. The different colors refer to the years 2005 to 2013 (see legend). (a) The NDIR CO<sub>2</sub> measurements vs. FTIR CO<sub>2</sub> measurements including both, the annual CO<sub>2</sub> increase and the seasonality; (b) as (a) but without seasonality; (c) as (a) but detrended; (d) as (a) but with neither annual CO<sub>2</sub> increase nor seasonality. The dashed line is the 1 : 1 line.

time shift with a maximum correlation of 0.495 at a time shift of 165 h, at lower and higher time shifts, the correlation is decreasing (Fig. 11c). The correlation of the detrended and deseasonalized data sets shows no distinct pattern and is oscillating around 0 (Fig. 11d).

Since the air volume measured by the FTIR is much bigger than the NDIR system's volume, vertical mixing and trans-

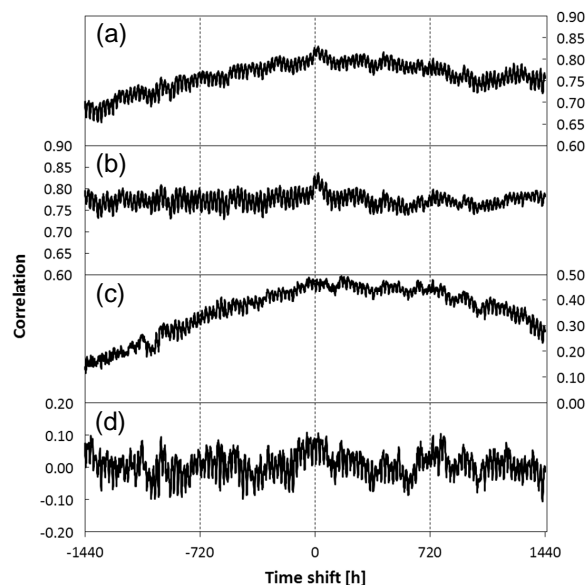


**Figure 11.** Evolution of the correlation between the filtered FTIR and NDIR data sets with changing time shift. (a) Correlation between complete data sets; (b) correlation between the two data sets without seasonality; (c) correlation between the two data sets without trend; (d) correlation between the two data sets with neither trend nor seasonality.

port processes can occur and thereby changing the CO<sub>2</sub> mole fraction in the measured air parcels. Therefore, moving averages with increasing widths (up to ±600 h) were calculated from the NDIR data and the obtained averaged NDIR values were correlated with the filtered FTIR data set. Changing the width of the moving average does not have a strong influence on the correlation between the two filtered data sets, because the increasing width of the moving average just smooths the data set. The correlation remains at about 0.85 (Fig. 12a), with a very small increase of the correlation at the beginning, most probably due to the above-mentioned smoothing effect. The same is true for the correlation between the deseasonalized data sets. They show a high correlation of about 0.84 over the whole range of widths, with a slight increase at the



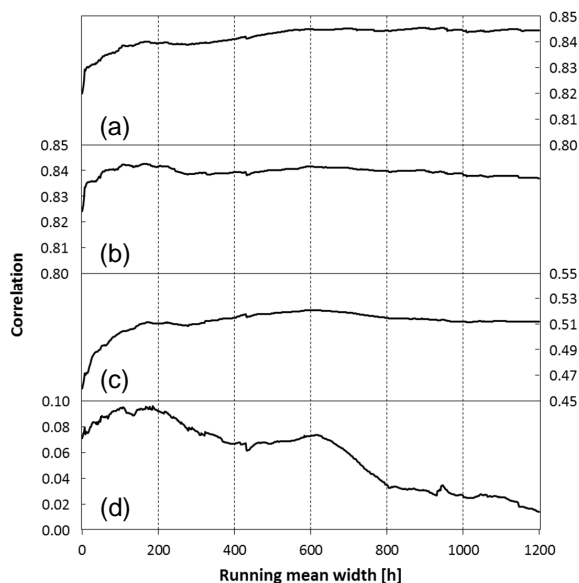


**Figure 12.** Change of the correlation between the filtered FTIR and NDIR data sets with increasing width of the running mean. (a) Correlation between the two data sets with seasonality and slope; (b) correlation between the two data sets without seasonality; (c) correlation between the two data sets without slope; (d) correlation between the two data sets with neither slope nor seasonality.

beginning, which is not significant (Fig. 12b). By detrending the data sets, the correlation is increasing with the width of the moving average and shows a plateau of higher correlation of about 0.5 at a width 150 to 600 h from where on it is decreasing again (Fig. 12c). However, the changes in the correlation within the range of 150 to 600 h are very small. The detrended and deseasonalized data sets show a very low correlation and the improvement of the correlation due to the changing width of the moving average is negligible. Over all, the improvement of the correlations due to the changing width of the moving average is very small (Fig. 12d).

Finally both, the time shift and the width of the moving average were varied about  $\pm 1440$  and  $\pm 600$  h, to see with which combination of time shift and width the best correlation can be reached. They all show a ridge of higher correlation at a time shift around zero, which is broadening with increasing width of the moving average, except for the data without slope and seasonality, which have a low correlation anyway (Fig. 13). The increasing width of the moving average leads to a small improvement of the correlations in the beginning; however, over all it does not seem to have a strong influence on the correlations. The time shift on the other hand has an influence on correlation between the complete filtered data sets and even more on the correlation of the detrended data sets. In the correlation of the deseasonalized data sets, the influence of the time shift is very limited except for the small ridge of slightly enhanced correlations around zero time shift as mentioned above.

## 4 Discussion

The filtered FTIR and NDIR data sets show a very similar increase in the  $\text{CO}_2$  mole fraction of ambient air, despite the two totally different measurement principles. The calculated annual  $\text{CO}_2$  trends of the FTIR and NDIR data sets are  $2.04 \pm 0.07$  and  $1.97 \pm 0.05$   $\text{ppm yr}^{-1}$ , respectively (Fig. 4) and are in good agreement with flask measurements done at JFJ with a slope of  $1.85$   $\text{ppm yr}^{-1}$  (van der Laan-Luijkx et al., 2013) and other remote stations in the Northern Hemisphere, for example, Mauna Loa with  $2.05$   $\text{ppm yr}^{-1}$  (NOAA, 2014) or Alert with  $1.85$   $\text{ppm yr}^{-1}$  (Keeling et al., 2001). Also the NDIR data set average seasonality of  $10.10 \pm 0.73$  ppm is in good agreement with the seasonality of these flask measurements, which were  $10.54 \pm 0.18$  ppm in the period 2007 to 2011 (van der Laan-Luijkx et al., 2013) and is roughly double the FTIR's average seasonality of  $4.46 \pm 1.11$  ppm (Fig. 5). The lower seasonality of the FTIR data set can be explained by the fact that the NDIR system is measuring  $\text{CO}_2$  mole fractions at the Sphinx Observatory, which is most of the time above the PBL (Henne et al., 2010) but still closer to the ground than the FTIR measurements. Therefore, the signal of the biosphere is stronger than in the column, where it is attenuated by vertical mixing and transport processes of the atmosphere with increasing height. Also the fixed a priori vertical  $\text{CO}_2$  profile may contribute partly to the lower seasonality of the FTIR measurements. The shape of the profile used to retrieve the  $\text{CO}_2$  data does not reproduce the changes due to seasonality and is therefore not always the optimum. By using a seasonally varying a priori retrieval the seasonality might be slightly higher because the amplitude of  $\text{CO}_2$  is better retrieved (Barthlott et al., 2015). Furthermore, in the tropopause and the lower stratosphere, the phase of the  $\text{CO}_2$  seasonality is shifted by several months (Bönisch et al., 2008, 2009; Gurk et al., 2008). However, this has only a minor influence on the observed dampening of the amplitude of the FTIR seasonality compared to the vertical mixing, since the stratosphere contains only about 10 % of the abundance of atmospheric air molecules.

It is not easy to define the seasonal minimum and maximum in the FTIR data set because they are not very clearly pronounced. By fitting a two harmonic function, the minimum was found to be in the middle of August, the maximum in the middle of January. While the minimum of the NDIR data set is around the same time, the maximum of the FTIR data set occurs roughly 10 weeks earlier than the maxima of the NDIR data set (Fig. 5). The timing of the minima of both data sets and the maximum of the NDIR data set coincide quite well with net land-atmosphere carbon flux changes from negative to positive values and vice versa (Zeng et al., 2014). Therefore, an alternative explanation is needed for the early maximum of the FTIR data set. Sensitivity analyses revealed that the upper tropospheric air originates from different geographic regions, mainly from the southwest, than the in situ air measured by the NDIR. During summer, the

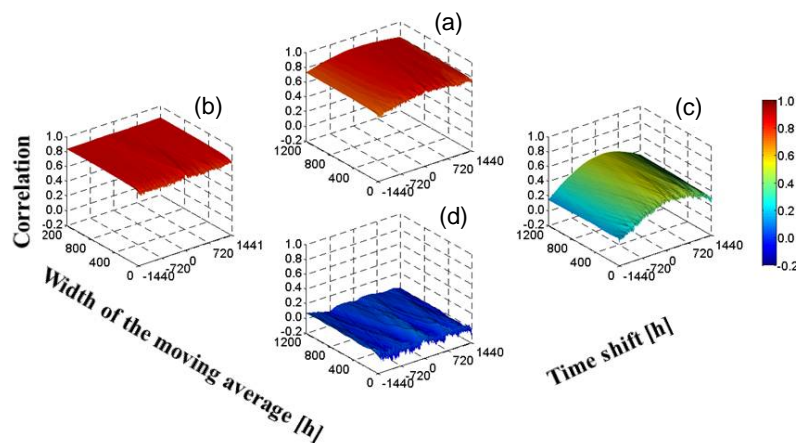


**Figure 13.** Surface plots of the correlation of the NDIR CO<sub>2</sub> measurements vs. the FTIR CO<sub>2</sub> measurements. The *x* axis corresponds to the time shift, the *y* axis to the width of the moving average and the *z* axis to the correlation between the FTIR and the NDIR data set, the color code illustrates the correlation and corresponds to the *z* axis values. (a) The FTIR CO<sub>2</sub> measurements vs. the corresponding NDIR CO<sub>2</sub> measurements including the annual CO<sub>2</sub> increase as well as the seasonality; (b) as (a) but without seasonality; (c) as (a) but detrended; (d) as (a) but detrended and deseasonalized.

NDIR measurements record mainly air from European regions, whereas the FTIR sees more influence from the west (Fig. 6). From winter to spring, NDIR CO<sub>2</sub> values are again driven by European sources, whereas FTIR values represent a significantly wider foot print reaching to west and further to the north in contrast to the summer situation (Figs. 7, 8). Similar studies investigating CO at JFJ also showed that JFJ is not only sensitive to central Europe but also to regions as far west as, for example, North America, the Pacific, or even Asia, and that the influence of these regions is getting stronger with increasing height (Dils et al., 2011; Pfister et al., 2004; Zellweger et al., 2009). Therefore, the air measured by the FTIR is partially decoupled from the increasing CO<sub>2</sub> values of the wintertime Northern Hemisphere. Furthermore, the decoupling might be amplified by the weak overturn of tropospheric air in winter. Towards spring, the tropospheric overturn speeds up again which results in synchronous CO<sub>2</sub> minima for both data sets in August (Fig. 9). Additionally, the phase of the stratosphere's seasonal cycle is shifted with respect to the tropospheric seasonal cycle because there is a time lag for tropospheric air reaching the stratosphere (Ray et al., 2014; Sawa et al., 2015, 2008). This effect is only seen by the column measurements of the FTIR system but not by the NDIR system and therefore possibly adds to the differences in the seasonalities of the two data sets. These findings can help one understand the shift in the observed wintertime maximum of CO<sub>2</sub> between FTIR (January) and NDIR (March–April). To model and quantify these effects properly is rather difficult and beyond the scope of this study, but could be investigated in a following study. The land surfaces of Northern Hemispheric mid-latitudes act as a net CO<sub>2</sub> source during the winter half year, since photosynthesis is largely reduced and respiration and anthropogenic emissions

of CO<sub>2</sub> dominate the budget. Hence, the maximum of CO<sub>2</sub> is observed at the end of the winter half year and close to the surface. For the free troposphere above JFJ as observed by the FTIR, the direct link to these wintertime releases of CO<sub>2</sub> is weakened due to generally reduced vertical transport. At the same time more frequent transport from and land surface contact in the tropics can be deduced (Fig. 9), an area that even during the winter half year may act as a net CO<sub>2</sub> sink due to photosynthetic uptake. An earlier onset of decreasing CO<sub>2</sub> in the free troposphere above JFJ could thereby be explained by different seasonality of transport and vertical mixing. Additionally, the assumption of a fixed a priori CO<sub>2</sub> vertical distribution to retrieve the column integrated CO<sub>2</sub> concentration from the FTIR data set may contribute partially to the observed shift of 10 weeks in the NDIR and FTIR maxima, because it is representing the distribution in winter/spring inadequately.

Another hint that the two systems are not measuring the same air parcels can be found in correlation analyses. After omitting outliers, which are mostly caused by synoptic events, thermal uplift of polluted air from surrounding valleys, or other local to regional transport events, the correlation of the two data sets is as large as 0.820, which is quite encouraging considering the different nature of the measurements. By excluding the seasonality from both data sets, the correlation stays almost the same (i.e., 0.824) but drops to 0.460 if the seasonality is included but the annual CO<sub>2</sub> increase is subtracted. The comparison of the two CO<sub>2</sub> data sets with the annual CO<sub>2</sub> increase and the seasonality subtracted showed a very low correlation of 0.071, which is negligible (Fig. 10). Because of possible delays and mixing effects of the CO<sub>2</sub> signal, the time shift as well as the width of the moving average calculated on the hourly val-

ues of the NDIR CO<sub>2</sub> values varied between  $\pm 1440$  and up to  $\pm 600$  h, respectively. Shifting the NDIR time relative to the FTIR measurement time creates a ridge of higher correlations around 0 h time shift with a slight tendency towards positive values (Fig. 13a). This ridge-like form is clearly pronounced in the correlation plot between the complete filtered FTIR and NDIR data sets and even more in the data sets without slope (Fig. 13c) than in the correlation of the data sets without seasonality (Fig. 13b). There it is very small and the correlation is high across the whole time shift and averaging width. The constantly high correlation for deseasonalized data sets is due to both data sets containing mostly background air, whose CO<sub>2</sub> mole fraction changes are mainly driven by the annual CO<sub>2</sub> increase and by the seasonality of the CO<sub>2</sub> signal. Since the larger of the two (the seasonality) is subtracted the high correlation is mainly driven by the slope, which was calculated to be the same within uncertainties and stays more or less constant over the examined period. Therefore, the time shift has almost no influence. The remaining fluctuations in the CO<sub>2</sub> mole fractions with higher frequencies than the seasonality seem to play a minor role, because they are almost not visible in the comparison of the data sets without seasonality except for the small ridge (Fig. 13b), or there is no correlation at all, as in the comparison of the two data sets without slope and seasonality (Fig. 13d). This is indicating that the two measurement systems are not measuring the same air parcels, even not with a certain delay, or that the CO<sub>2</sub> signal of the NDIR system, which is measured at the lower end of the FTIR column, becomes diluted beyond recognition for FTIR by the air mixing processes. The positive effect of the increasing width of the moving average on the correlation is strongest, but still very low, around the first 100 h. Afterwards its main effect is broadening the ridge of the slightly enhanced correlations. The reason for the broadening effect of the increasing width is its smoothing effect on the NDIR values. With increasing width, the influence of a specific NDIR point on the correlation becomes smaller and the NDIR data set evolves into a smooth sine-like curve with decreasing amplitudes, similar to the FTIR data set, where this form is caused by the higher sampling volume and the dampening due to mixing processes in the atmosphere. However, the small influence of the moving average's width on the correlation means that the correlation of the in situ and the column measurement is mainly influenced by the slope and the seasonality. Short-term fluctuations play a minor role mainly because either their CO<sub>2</sub> signal is dampened too much to be seen in the column measurement or it is not measured at all as, e.g., diurnal cycles because of the applied measurement methods.

## 5 Conclusions

Two data sets of CO<sub>2</sub> measurements at the High Altitude Research Station Jungfraujoch in the period 2005 to 2013 were

compared. The FTIR system is measuring the attenuation of solar light at different wavelengths caused by molecules of light absorbing gas species in the column between the Sphinx Observatory and the sun. From the obtained spectra, with the knowledge of CO<sub>2</sub> specific extinction bands and the pressure distribution along the path of the light, it is possible to calculate the CO<sub>2</sub> mole fraction in the column. The NDIR system is measuring the CO<sub>2</sub> mole fraction of ambient air at the Sphinx Observatory, which corresponds to the lower boundary of the FTIR measurements. The two data sets were filtered with a statistical approach to exclude CO<sub>2</sub> measurements, which were influenced by recent transport from the planetary boundary layer. The filtering caused a loss of about 5% in both, the NDIR and the FTIR data sets.

The annual CO<sub>2</sub> increase of the two data sets was calculated with a Monte Carlo approach. Despite an average offset of 13 ppm between the two data sets, which is within the systematic uncertainty affecting the FTIR measurement, the slopes were in good agreement, namely,  $2.04 \pm 0.07$  ppm yr<sup>-1</sup> in the FTIR measurements and  $1.97 \pm 0.05$  ppm yr<sup>-1</sup> in the NDIR data set. The seasonality of the CO<sub>2</sub> signal of the NDIR and the FTIR system is  $10.10 \pm 0.73$  and  $4.46 \pm 1.11$  ppm, respectively. The difference is caused by a dampening of the CO<sub>2</sub> signal with increasing altitude due to mixing processes. While the minima of the two data sets both occur in the simultaneously, the maxima of the FTIR data set was found 10 weeks earlier than the NDIR maxima.

The difference in the occurrence of the minima is most probably caused by the different transport history of the air masses measured at JFJ and in the column above JFJ. In January, the in situ system is measuring air from central Europe and the Mediterranean, whereas the air masses of the column measurements are more affected by the sub-tropic northern Atlantic. With the onset of spring in Europe, the photosynthetic activity is increasing and the CO<sub>2</sub> mole fraction of air measured by the in situ system starts to decrease at the end of March. The two filtered data sets as well as the two deseasonalized data sets show a high correlation, whereas the correlation between the two detrended data sets is only mediocre and inexistent between the two detrended and deseasonalized data sets. Neither shifting the time of the NDIR measurements relative to the FTIR measurements nor increasing the width of the moving average increased the correlation between the two data sets significantly. The enhanced correlation values around a time shift of zero indicates that (i) there is not a systematic time shift apparent and that (ii) the correlation between the two data sets is mainly driven by the annual CO<sub>2</sub> increase and to a lesser degree by the seasonality. Therefore, both measurement systems are suitable to measure the annual CO<sub>2</sub> increase, because this signal is well mixed within the atmosphere. Short-term variations as the seasonality or daily variations are less or not comparable, because (a) the transport history of the air parcels measured is different, (b) the signal is mixed beyond recognition, or



(c) since the FTIR has a low vertical sensitivity it was not exploited in the present retrievals and therefore the measured column signal contains mixed information from the troposphere and the stratosphere.

## 6 Data availability

Kup data can be downloaded from WMO's World Data Centre for Greenhouse Gases (<http://ds.data.jma.go.jp/gmd/wdcgg/>), the FTIR data are available as a Supplement.

**The Supplement related to this article is available online at doi:10.5194/acp-16-9935-2016-supplement.**

*Acknowledgements.* This work was financially supported by the Swiss National Science Foundation (SNF-Project 200020\_134641) and the Federal Office of Meteorology and Climatology MeteoSwiss in the framework of Swiss GCOS. We like to thank the International Foundation High Altitude Research Stations Jungfrauoch and Gornergrat (HFSJG), especially the custodians Martin Fischer, Felix Seiler and Urs Otz for changing the calibration gases cylinders of the NDIR system and other maintenance work. Additionally the authors like to thank Hanspeter Moret and Peter Nyfeler for his precious work and help in maintaining and repairing the systems in the Laboratory in Bern and also at Jungfrauoch. The Belgian contribution to the present work was mainly supported by the Belgian Science Policy Office (BELSPO) and the Fonds de la Recherche Scientifique – FNRS, both in Brussels. FLEXPART simulations were carried out in the framework of EC FP7 project NORS (grant agreement no. 284421). Additional support was provided by MeteoSwiss (GAW-CH) and the Fédération Wallonie Bruxelles. We are grateful to the many colleagues and collaborators, who have contributed to FTIR data acquisition.

Edited by: A. Engel

Reviewed by: two anonymous referees

## References

- Arrhenius, S.: XXXI. On the influence of carbonic acid in the air upon the temperature of the ground, *Philosophical Magazine Series 5*, 41, 237–276, doi:10.1080/14786449608620846, 1896.
- Baltensperger, U., Gäggeler, H. W., Jost, D. T., Lugauer, M., Schwikowski, M., Weingartner, E., and Seibert, P.: Aerosol climatology at the high-alpine site Jungfrauoch, Switzerland, *J. Geophys. Res.-Atmos.*, 102, 19707–19715, doi:10.1029/97JD00928, 1997.
- Barthlott, S., Schneider, M., Hase, F., Wiegeler, A., Christner, E., González, Y., Blumenstock, T., Dohe, S., García, O. E., Sepúlveda, E., Strong, K., Mendonca, J., Weaver, D., Palm, M., Deutscher, N. M., Warneke, T., Notholt, J., Lejeune, B., Mahieu, E., Jones, N., Griffith, D. W. T., Velasco, V. A., Smale, D., Robinson, J., Kivi, R., Heikkinen, P., and Raffalski, U.: Using XCO<sub>2</sub> retrievals for assessing the long-term consistency of NDACC/FTIR data sets, *Atmos. Meas. Tech.*, 8, 1555–1573, doi:10.5194/amt-8-1555-2015, 2015.
- Bender, M. L., Ho, D. T., Hendricks, M. B., Mika, R., Battle, M. O., Tans, P. P., Conway, T. J., Sturtevant, B., and Cassar, N.: Atmospheric O<sub>2</sub>/N<sub>2</sub> changes, 1993–2002: Implications for the partitioning of fossil fuel CO<sub>2</sub> sequestration, *Global Biogeochem. Cy.*, 19, GB4017, doi:10.1029/2004GB002410, 2005.
- Bönisch, H., Hoor, P., Gurk, C., Feng, W., Chipperfield, M., Engel, A., and Bregman, B.: Model evaluation of CO<sub>2</sub> and SF<sub>6</sub> in the extratropical UT/LS region, *J. Geophys. Res.-Atmos.*, 113, D06101, doi:10.1029/2007JD008829, 2008.
- Bönisch, H., Engel, A., Curtius, J., Birner, Th., and Hoor, P.: Quantifying transport into the lowermost stratosphere using simultaneous in-situ measurements of SF<sub>6</sub> and CO<sub>2</sub>, *Atmos. Chem. Phys.*, 9, 5905–5919, doi:10.5194/acp-9-5905-2009, 2009.
- Bousquet, P., Gaudry, A., Ciais, P., Kazan, V., Monfray, P., Simmonds, P. G., Jennings, S. G., and O'Connor, T. C.: Atmospheric CO<sub>2</sub> concentration variations recorded at Mace Head, Ireland, from 1992 to 1994, *Phys. Chem. Earth*, 21, 477–481, doi:10.1016/S0079-1946(97)81145-7, 1996.
- Brenninkmeijer, C. A. M., Crutzen, P., Boumard, F., Dauer, T., Dix, B., Ebinghaus, R., Filippi, D., Fischer, H., Franke, H., Frieß, U., Heintzenberg, J., Helleis, F., Hermann, M., Kock, H. H., Koepfel, C., Lelieveld, J., Leuenerberger, M., Martinsson, B. G., Miemczyk, S., Moret, H. P., Nguyen, H. N., Nyfeler, P., Oram, D., O'Sullivan, D., Penkett, S., Platt, U., Pupek, M., Ramonet, M., Randa, B., Reichelt, M., Rhee, T. S., Rohwer, J., Rosenfeld, K., Scharffe, D., Schlager, H., Schumann, U., Slemr, F., Sprung, D., Stock, P., Thaler, R., Valentino, F., van Velthoven, P., Waibel, A., Wandel, A., Waschitschek, K., Wiedensohler, A., Xueref-Remy, I., Zahn, A., Zech, U., and Ziereis, H.: Civil Aircraft for the regular investigation of the atmosphere based on an instrumented container: The new CARIBIC system, *Atmos. Chem. Phys.*, 7, 4953–4976, doi:10.5194/acp-7-4953-2007, 2007.
- Broecker, W. S. and Peng, T.-H.: *Tracers in the Sea*, Lamont-Doherty Geological Observatory, Palisades, New York, 1982.
- Buchwitz, M., de Beek, R., Noël, S., Burrows, J. P., Bovensmann, H., Schneising, O., Khlystova, I., Bruns, M., Bremer, H., Bergamaschi, P., Körner, S., and Heimann, M.: Atmospheric carbon gases retrieved from SCIAMACHY by WFM-DOAS: version 0.5 CO and CH<sub>4</sub> and impact of calibration improvements on CO<sub>2</sub> retrieval, *Atmos. Chem. Phys.*, 6, 2727–2751, doi:10.5194/acp-6-2727-2006, 2006.
- Buschmann, M., Deutscher, N. M., Sherlock, V., Palm, M., Warneke, T., and Notholt, J.: Retrieval of xCO<sub>2</sub> from ground-based mid-infrared (NDACC) solar absorption spectra and comparison to TCCON, *Atmos. Meas. Tech.*, 9, 577–585, doi:10.5194/amt-9-577-2016, 2016.
- Butz, A., Guerlet, S., Hasekamp, O., Schepers, D., Galli, A., Aben, I., Frankenberg, C., Hartmann, J. M., Tran, H., Kuze, A., Keppel-Aleks, G., Toon, G., Wunch, D., Wennberg, P., Deutscher, N., Griffith, D., Macatangay, R., Messerschmidt, J., Notholt, J., and Warneke, T.: Toward accurate CO<sub>2</sub> and CH<sub>4</sub> observations from GOSAT, *Geophys. Res. Lett.*, 38, L14812, doi:10.1029/2011GL047888, 2011.
- Chevallier, F., Maksyutov, S., Bousquet, P., Bréon, F.-M., Saito, R., Yoshida, Y., and Yokota, T.: On the accuracy of the CO<sub>2</sub> surface

- fluxes to be estimated from the GOSAT observations, *Geophys. Res. Lett.*, 36, L19807, doi:10.1029/2009GL040108, 2009.
- Chevallier, F., Ciais, P., Conway, T. J., Aalto, T., Anderson, B. E., Bousquet, P., Brunke, E. G., Ciattaglia, L., Esaki, Y., Fröhlich, M., Gomez, A., Gomez-Pelaez, A. J., Haszpra, L., Krummel, P. B., Langenfelds, R. L., Leuenberger, M., Machida, T., Maignan, F., Matsueda, H., Morguí, J. A., Mukai, H., Nakazawa, T., Peylin, P., Ramonet, M., Rivier, L., Sawa, Y., Schmidt, M., Steele, L. P., Vay, S. A., Vermeulen, A. T., Wofsy, S., and Worthy, D.: CO<sub>2</sub> surface fluxes at grid point scale estimated from a global 21 year re-analysis of atmospheric measurements, *J. Geophys. Res.-Atmos.*, 115, D21307, doi:10.1029/2010JD013887, 2010.
- Crisp, D., Atlas, R. M., Breon, F. M., Brown, L. R., Burrows, J. P., Ciais, P., Connor, B. J., Doney, S. C., Fung, I. Y., Jacob, D. J., Miller, C. E., O'Brien, D., Pawson, S., Randerson, J. T., Rayner, P., Salawitch, R. J., Sander, S. P., Sen, B., Stephens, G. L., Tans, P. P., Toon, G. C., Wennberg, P. O., Wofsy, S. C., Yung, Y. L., Kuang, Z., Chudasama, B., Sprague, G., Weiss, B., Pollock, R., Kenyon, D., and Schroll, S.: The Orbiting Carbon Observatory (OCO) mission, *Adv. Space Res.*, 34, 700–709, doi:10.1016/j.asr.2003.08.062, 2004.
- Dils, B., De Mazière, M., Müller, J. F., Blumenstock, T., Buchwitz, M., de Beek, R., Demoulin, P., Duchatelet, P., Fast, H., Frankenberg, C., Gloudemans, A., Griffith, D., Jones, N., Kerzenmacher, T., Kramer, I., Mahieu, E., Mellqvist, J., Mittermeier, R. L., Notholt, J., Rinsland, C. P., Schrijver, H., Smale, D., Strandberg, A., Straume, A. G., Stremme, W., Strong, K., Sussmann, R., Taylor, J., van den Broek, M., Velasco, V., Wagner, T., Warneke, T., Wiacek, A., and Wood, S.: Comparisons between SCIAMACHY and ground-based FTIR data for total columns of CO, CH<sub>4</sub>, CO<sub>2</sub> and N<sub>2</sub>O, *Atmos. Chem. Phys.*, 6, 1953–1976, doi:10.5194/acp-6-1953-2006, 2006.
- Dils, B., Cui, J., Henne, S., Mahieu, E., Steinbacher, M., and De Mazière, M.: 1997–2007 CO trend at the high Alpine site Jungfraujoch: a comparison between NDIR surface in situ and FTIR remote sensing observations, *Atmos. Chem. Phys.*, 11, 6735–6748, doi:10.5194/acp-11-6735-2011, 2011.
- Feely, R. A., Sabine, C. L., Lee, K., Berelson, W., Kleypas, J., Fabry, V. J., and Millero, F. J.: Impact of Anthropogenic CO<sub>2</sub> on the CaCO<sub>3</sub> System in the Oceans, *Science*, 305, 362–366, doi:10.1126/science.1097329, 2004.
- Gurk, Ch., Fischer, H., Hoor, P., Lawrence, M. G., Lelieveld, J., and Wernli, H.: Airborne in-situ measurements of vertical, seasonal and latitudinal distributions of carbon dioxide over Europe, *Atmos. Chem. Phys.*, 8, 6395–6403, doi:10.5194/acp-8-6395-2008, 2008.
- Halloran, P. R.: Does atmospheric CO<sub>2</sub> seasonality play an important role in governing the air-sea flux of CO<sub>2</sub>?, *Biogeosciences*, 9, 2311–2323, doi:10.5194/bg-9-2311-2012, 2012.
- Heinze, C., Maier-Reimer, E., and Winn, K.: Glacial pCO<sub>2</sub> Reduction by the World Ocean: Experiments With the Hamburg Carbon Cycle Model, *Paleoceanography*, 6, 395–430, doi:10.1029/91PA00489, 1991.
- Henne, S., Furger, M., and Prévôt, A. S. H.: Climatology of Mountain Venting–Induced Elevated Moisture Layers in the Lee of the Alps, *J. Appl. Meteorol.*, 44, 620–633, doi:10.1175/JAM2217.1, 2005.
- Henne, S., Brunner, D., Folini, D., Solberg, S., Klausen, J., and Buchmann, B.: Assessment of parameters describing representativeness of air quality in-situ measurement sites, *Atmos. Chem. Phys.*, 10, 3561–3581, doi:10.5194/acp-10-3561-2010, 2010.
- Henne, S., Steinbacher, M., Mahieu, E., Bader, W., Blumenstock, T., Cuevas-Agulló, E., Brunner, D., and Buchmann, B.: Comparison of ground-based remote sensing and in-situ observations of CO, CH<sub>4</sub> and O<sub>3</sub> accounting for representativeness uncertainty, *Geophys. Res. Abstr.*, EGU2013-9228, EGU General Assembly 2013, Vienna, Austria, 2013.
- Henne, S., Brunner, D., Oney, B., Leuenberger, M., Eugster, W., Bamberger, I., Meinhardt, F., Steinbacher, M., and Emmenegger, L.: Validation of the Swiss methane emission inventory by atmospheric observations and inverse modelling, *Atmos. Chem. Phys.*, 16, 3683–3710, doi:10.5194/acp-16-3683-2016, 2016.
- Heymann, J., Reuter, M., Hilker, M., Buchwitz, M., Schneising, O., Bovensmann, H., Burrows, J. P., Kuze, A., Suto, H., Deutscher, N. M., Dubey, M. K., Griffith, D. W. T., Hase, F., Kawakami, S., Kivi, R., Morino, I., Petri, C., Roehl, C., Schneider, M., Sherlock, V., Sussmann, R., Velasco, V. A., Warneke, T., and Wunch, D.: Consistent satellite XCO<sub>2</sub> retrievals from SCIAMACHY and GOSAT using the BESD algorithm, *Atmos. Meas. Tech.*, 8, 2961–2980, doi:10.5194/amt-8-2961-2015, 2015.
- IPCC: Climate Change 2013: The Physical Science Basis. Contribution of Working Group I to the Fifth Assessment Report of the Intergovernmental Panel on Climate Change, Cambridge University Press, Cambridge, United Kingdom and New York, NY, USA, 1535 pp., 2013.
- Karl, T. R. and Trenberth, K. E.: Modern Global Climate Change, *Science*, 302, 1719–1723, doi:10.1126/science.1090228, 2003.
- Keeling, C. D., Bacastow, R. B., Bainbridge, A. E., Ekdahl, C. A., Guenther, P. R., Waterman, L. S., and Chin, J. F. S.: Atmospheric carbon dioxide variations at Mauna Loa Observatory, Hawaii, *Tellus*, 28, 538–551, doi:10.1111/j.2153-3490.1976.tb00701.x, 1976.
- Keeling, C. D., Whorf, T. P., Wahlen, M., and van der Plichtt, J.: Interannual extremes in the rate of rise of atmospheric carbon dioxide since 1980, *Nature*, 375, 666–670, 1995.
- Keeling, C. D., Piper, S. C., Bacastow, R. B., Wahlen, M., Whorf, T. P., Heimann, M., and Meijer, H. A.: Exchanges of Atmospheric CO<sub>2</sub> and <sup>13</sup>CO<sub>2</sub> with the Terrestrial Biosphere and Oceans from 1978 to 2000. I. Global Aspects, SIO Reference Series, No. 01-06, Scripps Institution of Oceanography, San Diego, 28 pp., 2001.
- Komhyr, W. D., Gammon, R. H., Harris, T. B., Waterman, L. S., Conway, T. J., Taylor, W. R., and Thoning, K. W.: GLOBAL ATMOSPHERIC CO<sub>2</sub> DISTRIBUTION AND VARIATIONS FROM 1968–1982 NOAA GMCC CO<sub>2</sub> FLASK SAMPLE DATA, *J. Geophys. Res.-Atmos.*, 90, 5567–5596, doi:10.1029/JD090iD03p05567, 1985.
- Le Quéré, C., Peters, G. P., Andres, R. J., Andrew, R. M., Boden, T. A., Ciais, P., Friedlingstein, P., Houghton, R. A., Marland, G., Moriarty, R., Sitch, S., Tans, P., Arnett, A., Arvanitis, A., Bakker, D. C. E., Bopp, L., Canadell, J. G., Chini, L. P., Doney, S. C., Harper, A., Harris, I., House, J. I., Jain, A. K., Jones, S. D., Kato, E., Keeling, R. F., Klein Goldewijk, K., Körtzinger, A., Koven, C., Lefèvre, N., Maignan, F., Omar, A., Ono, T., Park, G.-H., Pfeil, B., Poulter, B., Raupach, M. R., Regnier, P., Rödenbeck, C., Saito, S., Schwinger, J., Segsneider, J., Stocker, B. D., Takahashi, T., Tilbrook, B., van Heuven, S., Viovy, N., Wankinkhof, R., Wiltshire, A., and Zaehle, S.: Global carbon budget

- 2013, *Earth Syst. Sci. Data*, 6, 235–263, doi:10.5194/essd-6-235-2014, 2014.
- Machida, T., Kita, K., Kondo, Y., Blake, D., Kawakami, S., Inoue, G., and Ogawa, T.: Vertical and meridional distributions of the atmospheric CO<sub>2</sub> mixing ratio between northern midlatitudes and southern subtropics, *J. Geophys. Res.-Atmos.*, 107, 8401, doi:10.1029/2001JD000910, 2002.
- Machida, T., Matsueda, H., Sawa, Y., Nakagawa, Y., Hirokuni, K., Kondo, N., Goto, K., Nakazawa, T., Ishikawa, K., and Ogawa, T.: Worldwide Measurements of Atmospheric CO<sub>2</sub> and Other Trace Gas Species Using Commercial Airlines, *J. Atmos. Ocean. Tech.*, 25, 1744–1754, doi:10.1175/2008JTECHA1082.1, 2008.
- Mahieu, E., Zander, R., Delbouille, L., Demoulin, P., Roland, G., and Servais, C.: Observed Trends in Total Vertical Column Abundances of Atmospheric Gases from IR Solar Spectra Recorded at the Jungfraujoch, *J. Atmos. Chem.*, 28, 227–243, doi:10.1023/A:1005854926740, 1997.
- Messenger, C., Schmidt, M., Ramonet, M., Bousquet, P., Simmonds, P., Manning, A., Kazan, V., Spain, G., Jennings, S. G., and Ciais, P.: Ten years of CO<sub>2</sub>, CH<sub>4</sub>, CO and N<sub>2</sub>O fluxes over Western Europe inferred from atmospheric measurements at Mace Head, Ireland, *Atmos. Chem. Phys. Discuss.*, 8, 1191–1237, doi:10.5194/acpd-8-1191-2008, 2008.
- Morino, I., Uchino, O., Inoue, M., Yoshida, Y., Yokota, T., Wennberg, P. O., Toon, G. C., Wunch, D., Roehl, C. M., Notholt, J., Warneke, T., Messerschmidt, J., Griffith, D. W. T., Deutscher, N. M., Sherlock, V., Connor, B., Robinson, J., Sussmann, R., and Rettinger, M.: Preliminary validation of column-averaged volume mixing ratios of carbon dioxide and methane retrieved from GOSAT short-wavelength infrared spectra, *Atmos. Meas. Tech.*, 4, 1061–1076, doi:10.5194/amt-4-1061-2011, 2011.
- NOAA: NOAA Earth System Research Laboratory, Global Monitoring Division, available at: <http://www.esrl.noaa.gov/gmd/ccgg/trends/>, last access: 30 October 2014.
- Oney, B., Henne, S., Gruber, N., Leuenberger, M., Bamberg, I., Eugster, W., and Brunner, D.: The CarboCount CH sites: characterization of a dense greenhouse gas observation network, *Atmos. Chem. Phys.*, 15, 11147–11164, doi:10.5194/acp-15-11147-2015, 2015.
- Pales, J. C. and Keeling, C. D.: The concentration of atmospheric carbon dioxide in Hawaii, *J. Geophys. Res.*, 70, 6053–6076, doi:10.1029/JZ070i024p06053, 1965.
- Pfister, G., Pétron, G., Emmons, L. K., Gille, J. C., Edwards, D. P., Lamarque, J. F., Attie, J. L., Granier, C., and Novelli, P. C.: Evaluation of CO simulations and the analysis of the CO budget for Europe, *J. Geophys. Res.-Atmos.*, 109, D19304, doi:10.1029/2004JD004691, 2004.
- Pollock, R., Haring, R. E., Holden, J. R., Johnson, D. L., Kapitaniuk, A., Mohlman, D., Phillips, C., Randall, D., Rechsteiner, D., Rivera, J., Rodriguez, J. I., Schwachert, M. A., and Sutin, B. M.: The Orbiting Carbon Observatory Instrument: performance of the OCO instrument and plans for the OCO-2 instrument, *Proc. SPIE 7826, Sensors, Systems, and Next-Generation Satellites XIV*, 78260W, doi:10.1117/12.865243, 2010.
- Ray, E. A., Moore, F. L., Rosenlof, K. H., Davis, S. M., Sweeney, C., Tans, P., Wang, T., Elkins, J. W., Bönisch, H., Engel, A., Sugawara, S., Nakazawa, T., and Aoki, S.: Improving stratospheric transport trend analysis based on SF<sub>6</sub> and CO<sub>2</sub> measurements, *J. Geophys. Res.-Atmos.*, 119, 14110–14128, doi:10.1002/2014JD021802, 2014.
- Revelle, R. and Suess, H. E.: Carbon Dioxide Exchange Between Atmosphere and Ocean and the Question of an Increase of Atmospheric CO<sub>2</sub> during the Past Decades, *Tellus*, 9, 18–27, doi:10.1111/j.2153-3490.1957.tb01849.x, 1957.
- Rothman, L. S., Jacquemart, D., Barbe, A., Chris Benner, D., Birk, M., Brown, L. R., Carleer, M. R., Chackerian, C., Chance, K., Coudert, L. H., Dana, V., Devi, V. M., Flaud, J.-M., Gamache, R. R., Goldman, A., Hartmann, J.-M., Jucks, K. W., Maki, A. G., Mandin, J.-Y., Massie, S. T., Orphal, J., Perrin, A., Rinsland, C. P., Smith, M. A. H., Tennyson, J., Tolchenov, R. N., Toth, R. A., Vander Auwera, J., Varanasi, P., and Wagner, G.: The HITRAN 2004 molecular spectroscopic database, *J. Quant. Spectrosc. Ra.*, 96, 139–204, doi:10.1016/j.jqsrt.2004.10.008, 2005.
- Sabine, C. L., Feely, R. A., Gruber, N., Key, R. M., Lee, K., Bullister, J. L., Wanninkhof, R., Wong, C. S., Wallace, D. W. R., Tilbrook, B., Millero, F. J., Peng, T.-H., Kozyr, A., Ono, T., and Rios, A. F.: The Oceanic Sink for Anthropogenic CO<sub>2</sub>, *Science*, 305, 367–371, doi:10.1126/science.1097403, 2004.
- Sawa, Y., Machida, T., and Matsueda, H.: Seasonal variations of CO<sub>2</sub> near the tropopause observed by commercial aircraft, *J. Geophys. Res.-Atmos.*, 113, D23301, doi:10.1029/2008JD010568, 2008.
- Sawa, Y., Machida, T., Matsueda, H., Niwa, Y., Tsuboi, K., Murayama, S., Morimoto, S., and Aoki, S.: Seasonal changes of CO<sub>2</sub>, CH<sub>4</sub>, N<sub>2</sub>O, and SF<sub>6</sub> in the upper troposphere/lower stratosphere over the Eurasian continent observed by commercial airliner, *Geophys. Res. Lett.*, 42, 2001–2008, doi:10.1002/2014GL062734, 2015.
- Schibig, M. F., Steinbacher, M., Buchmann, B., van der Laan-Luijkx, I. T., van der Laan, S., Ranjan, S., and Leuenberger, M. C.: Comparison of continuous in situ CO<sub>2</sub> observations at Jungfraujoch using two different measurement techniques, *Atmos. Meas. Tech.*, 8, 57–68, doi:10.5194/amt-8-57-2015, 2015.
- Sillén, L. G.: Regulation of O<sub>2</sub>, N<sub>2</sub> and CO<sub>2</sub> in the atmosphere; thoughts of a laboratory chemist, *Tellus*, 18, 198–206, doi:10.1111/j.2153-3490.1966.tb00226.x, 1966.
- Stohl, A., Forster, C., Frank, A., Seibert, P., and Wotawa, G.: Technical note: The Lagrangian particle dispersion model FLEXPART version 6.2, *Atmos. Chem. Phys.*, 5, 2461–2474, doi:10.5194/acp-5-2461-2005, 2005.
- Tans, P. P., Fung, I. Y., and Takahashi, T.: Observational Constraints on the Global Atmospheric CO<sub>2</sub> Budget, *Science*, 247, 1431–1438, doi:10.1126/science.247.4949.1431, 1990.
- Thompson, D. R., Chris Benner, D., Brown, L. R., Crisp, D., Malathy Devi, V., Jiang, Y., Natraj, V., Oyafuso, F., Sung, K., Wunch, D., Castaño, R., and Miller, C. E.: Atmospheric validation of high accuracy CO<sub>2</sub> absorption coefficients for the OCO-2 mission, *J. Quant. Spectrosc. Ra.*, 113, 2265–2276, doi:10.1016/j.jqsrt.2012.05.021, 2012.
- Thoning, K. W., Tans, P. P., and Komhyr, W. D.: Atmospheric carbon dioxide at Mauna Loa Observatory: 2. Analysis of the NOAA GMCC data, 1974–1985, *J. Geophys. Res.-Atmos.*, 94, 8549–8565, doi:10.1029/JD094iD06p08549, 1989.
- Trolier, M., White, J. W. C., Tans, P. P., Masarie, K. A., and Gemery, P. A.: Monitoring the isotopic composition of atmospheric CO<sub>2</sub>: Measurements from the NOAA Global Air Sam-



- pling Network, *J. Geophys. Res.-Atmos.*, 101, 25897–25916, doi:10.1029/96JD02363, 1996.
- Uglietti, C., Leuenberger, M., and Brunner, D.: European source and sink areas of CO<sub>2</sub> retrieved from Lagrangian transport model interpretation of combined O<sub>2</sub> and CO<sub>2</sub> measurements at the high alpine research station Jungfraujoch, *Atmos. Chem. Phys.*, 11, 8017–8036, doi:10.5194/acp-11-8017-2011, 2011.
- van der Laan-Luijkx, I. T., van der Laan, S., Uglietti, C., Schibig, M. F., Neubert, R. E. M., Meijer, H. A. J., Brand, W. A., Jordan, A., Richter, J. M., Rothe, M., and Leuenberger, M. C.: Atmospheric CO<sub>2</sub>, δ(O<sub>2</sub>/N<sub>2</sub>) and δ<sup>13</sup>CO<sub>2</sub> measurements at Jungfraujoch, Switzerland: results from a flask sampling intercomparison program, *Atmos. Meas. Tech.*, 6, 1805–1815, doi:10.5194/amt-6-1805-2013, 2013.
- Vigouroux, C., Blumenstock, T., Coffey, M., Errera, Q., García, O., Jones, N. B., Hannigan, J. W., Hase, F., Liley, B., Mahieu, E., Mellqvist, J., Notholt, J., Palm, M., Persson, G., Schneider, M., Servais, C., Smale, D., Thölix, L., and De Mazière, M.: Trends of ozone total columns and vertical distribution from FTIR observations at eight NDACC stations around the globe, *Atmos. Chem. Phys.*, 15, 2915–2933, doi:10.5194/acp-15-2915-2015, 2015.
- Wunch, D., Toon, G. C., Blavier, J.-F. L., Washenfelder, R. A., Notholt, J., Connor, B. J., Griffith, D. W. T., Sherlock, V., and Wennberg, P. O.: The Total Carbon Column Observing Network, *Philos. T. R. Soc. Lond. A*, 369, 2087–2112, doi:10.1098/rsta.2010.0240, 2011.
- Yokota, T., Yoshida, Y., Eguchi, N., Ota, Y., Tanaka, T., Watanabe, H., and Maksyutov, S.: Global Concentrations of CO<sub>2</sub> and CH<sub>4</sub> Retrieved from GOSAT: First Preliminary Results, *SOLA*, 5, 160–163, doi:10.2151/sola.2009-041, 2009.
- Zander, R., Mahieu, E., Demoulin, P., Duchatelet, P., Roland, G., Servais, C., Mazière, M. D., Reimann, S., and Rinsland, C. P.: Our changing atmosphere: Evidence based on long-term infrared solar observations at the Jungfraujoch since 1950, *Sci. Total Environ.*, 391, 184–195, doi:10.1016/j.scitotenv.2007.10.018, 2008.
- Zellweger, C., Ammann, M., Buchmann, B., Hofer, P., Lugauer, M., Rüttimann, R., Streit, N., Weingartner, E., and Baltensperger, U.: Summertime NO<sub>y</sub> speciation at the Jungfraujoch, 3580 m above sea level, Switzerland, *J. Geophys. Res.-Atmos.*, 105, 6655–6667, doi:10.1029/1999JD901126, 2000.
- Zellweger, C., Forrer, J., Hofer, P., Nyeki, S., Schwarzenbach, B., Weingartner, E., Ammann, M., and Baltensperger, U.: Partitioning of reactive nitrogen (NO<sub>y</sub>) and dependence on meteorological conditions in the lower free troposphere, *Atmos. Chem. Phys.*, 3, 779–796, doi:10.5194/acp-3-779-2003, 2003.
- Zellweger, C., Hüglin, C., Klausen, J., Steinbacher, M., Vollmer, M., and Buchmann, B.: Inter-comparison of four different carbon monoxide measurement techniques and evaluation of the long-term carbon monoxide time series of Jungfraujoch, *Atmos. Chem. Phys.*, 9, 3491–3503, doi:10.5194/acp-9-3491-2009, 2009.
- Zeng, N., Zhao, F., Collatz, G. J., Kalnay, E., Salawitch, R. J., West, T. O., and Guanter, L.: Agricultural Green Revolution as a driver of increasing atmospheric CO<sub>2</sub> seasonal amplitude, *Nature*, 515, 394–397, doi:10.1038/nature13893, 2014.